1-1-2020

A Self-Assembled CO2 Reduction Electrocatalyst: Posy-Bouquet-Shaped Gold-Polyaniline Core-Shell Nanocomposite

Amruthalakshmi Vijayakumar
University of Wollongong, av644@uowmail.edu.au

Yong Zhao

Jinshuo Zou
University of Wollongong, jz940@uowmail.edu.au

Kezhong Wang
University of Wollongong, kw743@uowmail.edu.au

Chong Yong Lee
University of Wollongong, cylee@uow.edu.au

See next page for additional authors

A Self-Assembled CO2 Reduction Electrocatalyst: Posy-Bouquet-Shaped Gold-Polyaniline Core-Shell Nanocomposite

Abstract

© 2020 Wiley-VCH GmbH Here it was demonstrated that the decoration of gold (Au) with polyaniline is an effective approach in increasing its electrocatalytic reduction of CO2 to CO. The core-shell-structured gold-polyaniline (Au−PANI) nanocomposite delivered a CO2-to-CO conversion efficiency of 85 % with a high current density of 11.6 mA cm−2. The polyaniline shell facilitated CO2 adsorption, and the subsequent formation of reaction intermediates on the gold core contributed to the high efficiency observed.

Keywords

co2, reduction, electrocatalyst:, self-assembled, posy-bouquet-shaped, nanocomposite, gold-polyaniline, core-shell

Disciplines

Engineering | Physical Sciences and Mathematics

Publication Details

Vijayakumar, A., Zhao, Y., Zou, J., Wang, K., Lee, C., MacFarlane, D., Wang, C. & Wallace, G. (2020). A Self-Assembled CO2 Reduction Electrocatalyst: Posy-Bouquet-Shaped Gold-Polyaniline Core-Shell Nanocomposite. ChemSusChem, Online First

Authors

Amruthalakshmi Vijayakumar, Yong Zhao, Jinshuo Zou, Kezhong Wang, Chong Yong Lee, Douglas MacFarlane, Caiyun Wang, and Gordon G. Wallace

FULL PAPER

A Self-Assembled CO_2 Reduction Electrocatalyst: Posy-Bouquet-Shaped Gold-Polyaniline Core-Shell Nanocomposite

Amruthalakshmi Vijayakumar [a], Yong Zhao [a], Jinshuo Zou [a], Kezhong Wang [a], Chong-Yong Lee [a], Douglas R. McFarlane [b], Caiyun Wang *[a], Gordon G. Wallace *[a]

[a] A. Vijayakumar, Dr. Y. Zhao, J. Zou, K. Wang, Dr. C.Y. Lee, A/Prof. C. Wang, Prof. G. G. Wallace
ARC Centre of Excellence for Electromaterials Science,
Intelligent Polymer Research Institute
AIIM Facility, University of Wollongong,
North Wollongong, NSW 2500, Australia
E-mail: caiyun@uow.edu.au; gwallace@uow.edu.au
[b] Prof. D. R. McFarlane
School of Chemistry,
Monash University,
Clayton, VIC 3800, Australia

Supporting information for this article is given via a link at the end of the document.

Abstract: Here we demonstrate that the decoration of gold (Au) with polyaniline is an effective approach in increasing its electrocatalytic reduction of CO_2 to CO. The core-shell structured gold-polyaniline (Au-PANI) nanocomposite delivers a CO_2-to-CO conversion efficiency of 85% with a high current density of 11.6 mA cm^{-2}. The polyaniline shell facilitates CO_2 adsorption and the subsequent formation of reaction intermediates on the gold core contributes to the high efficiency observed.

Introduction

Carbon dioxide (CO_2), a by-product from fossil fuel combustion, is regarded as the primary greenhouse gas causing global warming. Currently, atmospheric CO_2 concentration has reached its highest level in recorded history at 410 ppm. [1] There is an urgent need to reduce CO_2 emissions, as well as recycle it as a source for producing valuable fuel and chemical feedstocks via photochemical[2], biochemical[3], thermochemical[4] and electrochemical methods.[5] Among them, the CO_2 electrochemical reduction (CO_2ER) is promising when considering its scalability and operation at ambient conditions.[6] Moreover, this process may be realized by utilizing renewable power sources from solar, wind and tide, which offers the potential for it to be part of a carbon-neutral energy cycle when combined with a carbon capture process. [7] Scalable and efficient electrocatalysts hold the key for the practical implementation of CO_2ER, in particular to overcome the challenges of sluggish kinetics and poor selectivity versus the H_2 evolution reaction (HER) that arises from the thermodynamic stability of CO_2.[8]

Gold is one of the best catalysts for the electrochemical CO_2-to-CO conversion, which is attributed to the fast conversion of CO_2 to *COOH via the strong *COOH binding, and the weak binding of *CO reaction intermediate facilitates the desorption of CO from its surface.[9] Different strategies have been employed to enhance its catalytic performance such as tuning the surface morphology[10], engineering the surface [9, 11], and alloying with other metals.[12] The integration of Au with a functional conductive support to form a composite is an efficient surface engineering approach, as the synergistic interaction between the metallic catalytic centre and conductive support facilitates charge transfer and promotes CO_2 activation and conversion.[13]

Nanocarbons and conducting polymers are two of the most commonly used supports for metal-based catalysts. For example, copper nanoparticles on pyridinic N-rich graphene (p-NG-Cu) displayed a 19% Faradaic Efficiency (FE) with respect to the formation of C_2H_4 at -0.9 V vs. RHE (Reversible Hydrogen Electrode).[14] The presence of Lewis base in the p-NG-Cu catalyst structure promoted proton/hydrogen aggregation around Cu, facilitating the conversion of CO_2 to C_2H_4. The use of silver nanowires (Ag NWs) as part of a carbon composite enabled a tunable production of H_2/CO for syngas generation.[15] Ultra-small gold nanoparticles (Au NPs) supported on reduced graphene oxide (rGO) nanosheets demonstrated an improved CO_2-to-CO conversion efficiency compared to pristine Au NPs.[16] Cobalt-polypyrrole particles immobilized on carbon black have been shown to utilize the hybridization of metal and organic materials to enhance the catalytic activity of the electroactive metallic centre in the conversion of CO_2-to-CO.[13c]

Polyaniline (PANI) is a common conducting polymer having strong electron donating amine groups and pi-conjugation across the polymer backbone.[17] Nanostructured PANI possesses the properties of a low-dimensional organic conductor with high surface area. Incorporating PANI with metal NPs can lower the activation energy for CO_2 reduction by effectively trapping the reactant due to the Lewis acid-base interaction between metal NPs/PANI and CO_2.[18] For example, the use of a Pd/PANI catalyst demonstrated a CO_2-to-HCOOH conversion with a FE of 22% in 0.5 M H_2SO_4 (-1.1 V vs. RHE).[19] Introducing a third component, carbon nanotubes (CNT), to form Pd-PANI/CNT composite further improved this conversion efficiency to 83 % at -0.163 V vs. RHE, as CNT promoted charge transport.[20] The use of Cu_2O NPs immobilized on PANI enabled conversion of CO_2 to formic acid and acetic acid in 0.1 M tetrabutylammonium perchlorate and methanol electrolyte.[21] The Sn-PANI film coated on nickel foam

demonstrated a good conversion of CO_2 to formate in 0.1 M potassium bicarbonate.[22] All these composites take advantage of the role that PANI can play in proton shuttling and outer sphere co-ordination effects through the conjugated backbone and the amino groups present. Au-PANI nanocomposites have demonstrated good catalytic capability for oxygen reduction reaction due to the enhanced oxophilicity of Au.[23] However, the use of Au-PANI nanocomposites as a catalyst for the CO_2ER has not been reported yet.

The syntheses of metal-PANI nanocomposites commonly involve multi-step processes and/or the use of strong reducing agents and surfactants that may affect the catalytic activity [24]. Herein we adopt a single-step ecofriendly approach that does not use any reducing agents or surfactants [25]. The direct redox reaction between aniline and gold salt at ambient conditions creates shape-tailored Au-PANI nanocomposites. These nanocomposites exhibit posy-bouquet-like morphology with excellent catalytic capability for the CO_2-to-CO conversion: a FE of 85% with a high partial current density of 11.6 mA cm^{-2} (mass activity = 23.2 A g^{-1}) at -0.9 V vs. RHE in 0.1 M $KHCO_3$; which is much higher than that of Au NPs. The selectivity dropped to only 23% after carbonizing the PANI layer to amorphous carbon. This work clearly demonstrates the active role of PANI layer in the Au-PANI composite on the catalytic ability for the CO_2ER. Also, it highlights the influence of gold content on the morphology of composite and the CO_2ER performance.

Results and Discussion

The formation of Au-PANI nanocomposites is illustrated schematically in Figure 1a. $HAuCl_4$ enables dissolution of aniline with subsequent oxidation to polyaniline with consistent reduction of $AuCl_4^-$ to Au°. Nanoparticles consisting of polyaniline and Au° are formed. Anisotropic growth of Au branches proceeded to form buds on the posy bouquet due to the different diffusion rates of Au through PANI and partial dissolution of PANI oligomer on Au promotes the faster growth of stems. Further agglomeration was prevented by the diffusion controlled mechanism through π-π interaction between the PANI aromatic rings on the Au[23b]. The newly formed nuclei underwent Ostwald ripening in the following stages as part of the surface energy minimization, and formed the self-assembled 3D hierarchical structure of Au-PANI nanocomposites through the molecular interaction between early formed nuclei[26]. The redox processes between aniline monomer and chloroauric acid were responsible for the self-assembly forming Au-PANI nanocomposites.

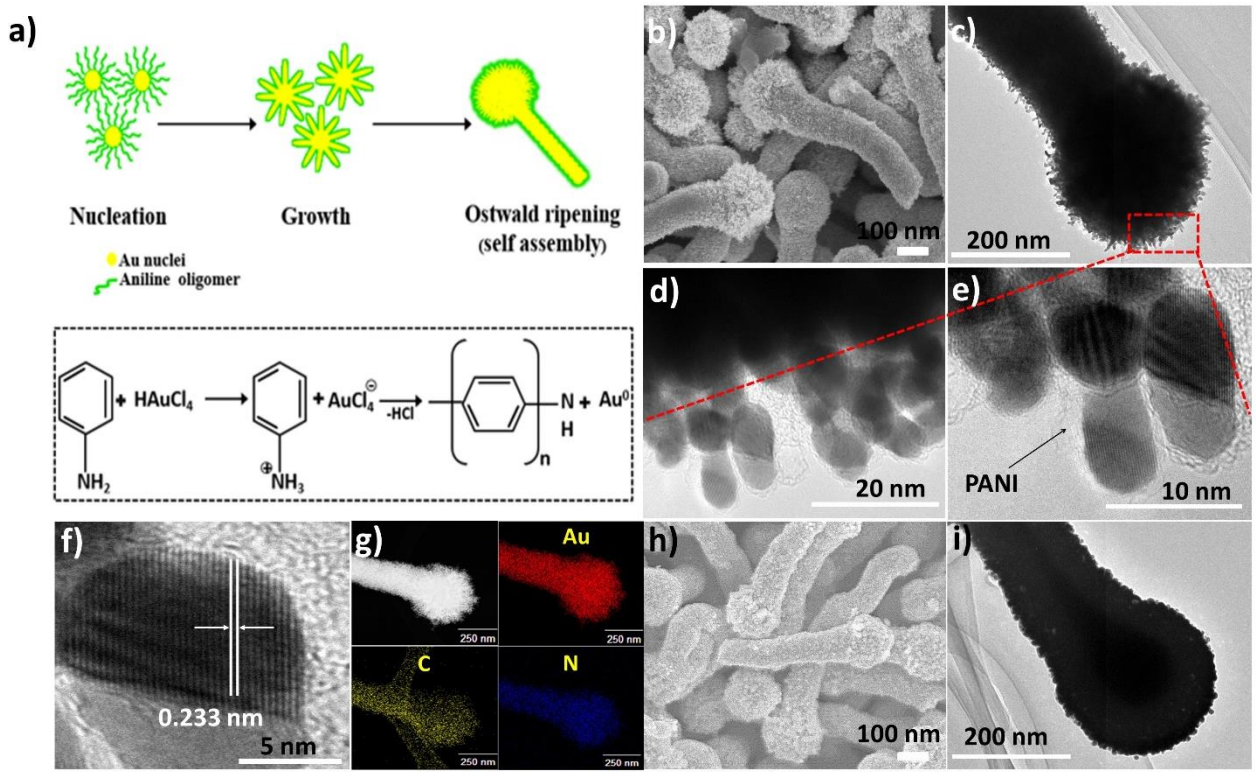

Figure 1. Synthesis and morphology of Au-PANI nanocomposite. a) Schematic illustration of the formation process of Au-PANI nanocomposite; b-f) SEM and TEM images of Au-$PANI_1$ nanocomposite; g) HAADF-STEM and STEM elemental mapping results of Au-$PANI_1$ nanocomposite; h-i) SEM and TEM images of Au-NC nanocomposite.

The Au-PANI composite displayed a posy bouquet like morphology for Au-$PANI_1$ (a molar ratio of 1:1 between $HAuCl_4$ and aniline monomer) (Figure 1b, c). This structure was further confirmed by high magnification TEM images (Figure 1c-f). It had a flowery head with a diameter of ~320 nm along with a stem of ~510 nm. The flowery head contained many fluffy buds with an average length of 15 nm. PANI uniformly wrapped the gold core in bouquet structure with well-defined boundary. The co-existence of Au nanostructures and PANI was confirmed by the HRTEM image (Figure 1e). The spacing between lattice fringes was 0.233

nm, attributing to the (111) plane of face-centred cubic (fcc)-Au (Figure 1f). The uniform distribution of elements Au, C and N along the posy bouquet structure was revealed by the STEM energy-dispersive X-ray spectroscopy (EDS) mapping (Figure 1g). The influence of the molar ratio of reactants on the morphology of Au-PANI nanostructures was also investigated. Au-PANI nanocomposites with different compositions were synthesized by keeping the same content of aniline monomer but changing the molar concentration of $HAuCl_4$. These products were referred to as Au-$PANI_1$, Au-$PANI_2$, and Au-$PANI_3$, and those numbers indicated the molar ratio between gold and aniline. When the ratio of $HAuCl_4$ to aniline increased from 1:1 to 2:1 and 3:1, the produced nanocomposites retained similar posy bouquet morphology (Figure SI 1a-f, Supplementary Information) with similar head size but with elongated stem: it was 0.6± 0.02 µm, 1.3 ± 0.03 µm and 2.3 ± 0.01 µm for Au-$PANI_1$, Au-$PANI_2$ and Au-$PANI_3$, respectively. This may be attributed to the fast growth of Au nanostructures that arose from dissolution of PANI oligomer at low concentration of aniline[27]. More fluffy buds were observed on Au-$PANI_1$ (Figure 1g). These results clearly demonstrate that the ratio between $HAuCl_4$ and aniline did impact on the formation of Au-PANI nanocomposites. After the annealing treatment, the same morphology of bouquet was retained for Au-NC but, the fluffy buds on the flowery head became shrunken as revealed in the SEM and TEM images (Figure 1h, i,). This may be explained by the carbonisation of PANI. Pure gold nanoparticles and polyaniline were synthesized as control samples. Those Au NPs were almost spherical with an average diameter of ~10 nm (Figure SI 1g), and the 0.233 nm spacing of fringes corresponds to the (111) plane of face-centred cubic (fcc)-Au (Figure SI 1h). PANI showed a nanoribbon morphology with an average width of 30 nm (Figure SI 1i).

The crystallinity and chain packing of Au-PANI composites were examined by XRD analysis, and the formation of Au-PANI composite was confirmed (Figure 2a, Figure S2a). Four sharp diffraction peaks appeared at 38°, 44°, 65° and 78° corresponding to the Bragg's reflections from (111), (200), (220) and (311) planes of Au (JCPDS 04-0784). They reveal the formation of fcc crystalline structure of Au in the composite. The highest intensity diffraction peak of Au (111) plane suggests the prominent growth of Au nanostructure along the lowest energy (111) facet. Pristine PANI and Au-PANI composite all displayed a peak at around 26° (inset of Figure 2a), which can be ascribed to the periodicity in parallel and perpendicular directions of the polymer chains of PANI. [28]

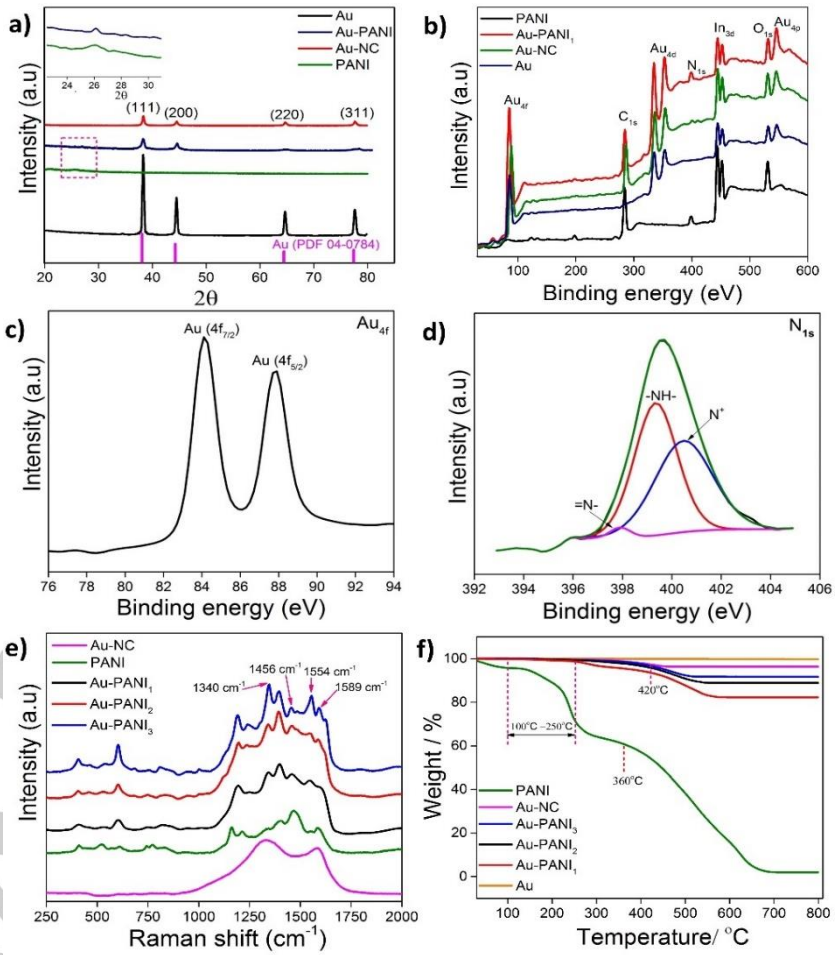

Figure 2. Structural characterizations of samples. a) XRD patterns of Au-$PANI_1$, Au-NC, PANI and Au; b) XPS survey scans of PANI, Au-NC, Au and Au-$PANI_1$; c) Core level spectra of Au 4f; d) N1s in Au-PANI composite; e) Raman spectra of Au-PANI nanocomposites, pure PANI and Au-NC; and f) TGA curves of Au-PANI nanocomposites, Au, Au-NC and PANI.

Elemental composition and the electronic state of Au in Au-PANI nanocomposite were analyzed by high resolution XPS. The XPS spectra (Figure 2b, Figure S2b) confirmed the presence of elements Au, C and N as expected. Compared with the spectrum of pure PANI, a new peak at 86.8 eV corresponding to Au 4f was observed for Au-PANI and Au-NC nanocomposites. The core level spectra (Figure 2c) of Au 4f showed two peaks at binding energies of 83.92 eV and 87.62 eV, assigned to the doublets of $4f_{7/2}$ and $4f_{5/2}$, respectively. This confirms the presence of zero valent gold (Au^o) in Au-PANI nanocomposite. The N1s core level spectrum (Figure 2d) revealed the presence of three different electronic states: quinoid imine (=N-), benzenoid amine (-NH-) and nitrogen cationic radical (N+) at binding energies of 398.4 eV, 399.5 eV and 401.1 eV, respectively; which matches well with the previous reports for PANI. [29] The core level spectrum of N1s in PANI-Au displayed a higher binding energy peak (400.6 eV) in comparison to that in PANI (400 eV) (Figure S2c). While the Au 4f spectrum in shifted to a lower binding energy compared to pure gold (Figure S2d). These results revealed a significant chemical interaction between gold and polyaniline where a strong bond was formed via the charge transfer process with PANI and gold nanoparticles as donor and acceptor, respectively.[30]

Raman spectra of PANI, Au-NC and different Au-PANI nanocomposites over the range of 2000 cm^{-1} to 200 cm^{-1} are shown in Figure 2e. For PANI, peaks at 1589 cm^{-1} and 1554 cm^{-1} represent the C-C stretching vibration in quinonoid ring and N-H deformation vibration in semi-quinonoid units, respectively. Peaks at 1456 cm^{-1} and 1340 cm^{-1} can be attributed to the C-N stretching vibration in the quinonoid structure, the $C–N^+$ vibration of delocalized polaronic structure[31] respectively. The C–N stretching vibrations of different benzenoid, quinonoid or polaronic forms and benzene ring deformations can be matched to the peak at 1241 cm^{-1}. Raman intensities of all these characteristic peaks of Au-PANI were significantly increased when compared to pure PANI. This can be attributed to the surface enhanced Raman scattering (SERS) effect due to the increased roughness of Au NPs and the enabling of easy charge transfer after forming nanocomposites[32]. For Au-NC, the peaks at 1350 cm^{-1} and 1580 cm^{-1} represent the disorder band (D) and graphitic band (G), respectively.

Thermal stability of Au-PANI nanocomposite, Au, Au-NC and PANI was analyzed by using TGA in air atmosphere (Figure 2f). For PANI and Au-PANI composites, a small weight loss was observed below 100 °C due to the expulsion of absorbed water; the slow weight loss from 100 to 250 °C can be attributed to the removal of PANI oligomers. Over the range from ~360 to 420 °C, they all displayed a rapid weight loss process, which may be caused by the oxidative decomposition of polymer backbone. The negligible weight loss for Au-NC and Au indicates their thermal stability in the air. Based on the thermal stability profile, the content of Au in Au-$PANI_1$, Au-$PANI_2$, Au-$PANI_3$ were estimated as 82%, 88%, and 91% respectively. These contents were higher than the theoretical values of 52%, 69% and 77% calculated from the reactants in the reaction. This may be explained by the dissolution of short chain PANI oligomers in the reaction mixture and the limited growth of PANI chain at relatively low Au content[27]. The amount of Au in Au-NC composites was 97%. Moreover, for those Au-PANI composites, the onset temperature of thermal degradation shifted to a higher degree by ~60 °C compared to that of pure PANI, indicating a higher thermal stability due to the strong interaction between PANI and Au nanoparticles [33].

The CO_2ER performance on Au, PANI, Au-PANI and Au-NC catalysts were first assessed by linear sweep voltammetry (LSV) studies (Figure 3a). All the Au containing catalysts exhibited much higher current densities and more positive onset potentials compared to PANI in CO_2-saturated 0.1 M $KHCO_3$, much higher LSV currents compared to that in argon (Ar)- saturated electrolyte (Figure S3). Specifically, all Au-PANI nanocomposites show low onset potentials of -0.3 V vs. RHE, which was favorable compared to Au (-0.4 V) and Au-NC (-0.5 V). These results give an initial indication about the positive impact of the interaction between Au and PANI and influencing the CO_2ER ability.

We further examined the CO_2ER performance by a series of controlled-potential electrolysis experiments. The iR-corrected total current densities showed similar trends to the LSV results (Figure 3b, Figure S4). Au-$PANI_1$, Au-$PANI_2$ and Au-$PANI_3$ displayed similar total current densities during the CO_2 reduction process; they were all higher than that of Au NPs and Au-NC. It confirms that PANI played an important role in the CO_2 reduction on these composite electrodes. The products generated were H_2 and CO. The faradaic efficiency (FE) of CO on all Au-PANI electrodes displayed a volcano-like behavior in the applied potential range. It reached a maximum FE at -0.9 V (corresponding to an overpotential of 790 mV for CO formation) (Figure 3c).

Au NPs displayed a different trend from those for Au-PANI samples. A higher FE_{CO} was observed from -0.5 V to -0.6 V due to high intrinsic activity of Au nanoparticles for CO_2-to-CO conversion. This may be ascribed to the the strong binding of reaction intermediate COOH* at the catalytic sites. The decreased CO formation efficiency from -0.7 V to -1.1 V (Figure S5a) may be attributed high coverage of *H intermediate and poor stability of *COOH intermediate on the catalytic sites under more negative cathodic potential. Such phenomenon has been previously reported.[10a, 34] The catalyst PANI alone merely generated H_2 over the whole range of applied potentials, consistent with the previous reports.[18] Au-PANI composites showed enhanced CO_2ER performance at the more negative potential range, from -0.7 to -1.1V, and reached a maximum faradaic efficiency of CO formation at -0.9 V. This may be attributed to the increased stability of reaction intermediate. Influence of PANI was further confirmed by the controlled potential experiments on Au-NC, a carbonized PANI structure. It displayed a faradaic efficiency of only 23% for CO formation at -0.9 V, much lower than that of 85% on Au-$PANI_2$. Therefore, this confirms that the presence of PANI on gold improved the CO_2 electroreduction performance.

Among all the examined Au-PANI composite electrodes, Au-$PANI_2$ exhibited the highest FE_{CO} by over ~10% compared to Au-$PANI_1$ at the potentials more negative than -0.7 V. Specifically, at -0.9 V the FE_{CO} was 85%, higher than that for Au-$PANI_1$ (70%) and Au-$PANI_3$ (79%) At -0.7 V, Au-$PANI_2$ displayed a FE_{CO} of 68%, higher or comparable to that exhibited (~60%) by carbon black-AuNP composite electrodes[10a] and ultrathin Au nanowires (~65%) with dominant edge reactive sites.[10c] The difference in catalytic performance on these three Au-PANI electrodes may be attributed to the utilization of an optimal Au and PANI content in

the composite. As the molar ratio of gold to aniline increased from 1 to 2, the composite showed a FE_{CO} increase by ~15%. The increased FE_{CO} may be explained by the effective interaction between Au and PANI, which is responsible for the absorption of CO_2 molecules and the subsequent conversion and product desorption. It may also explain the decreased FE_{CO} by 5% when the molar ratio was further increased to 3.

The excellent electrocatalytic ability of Au-PANI electrodes for reducing CO_2 was further verified by the increased geometric CO partial current density (j_{CO}) compared to Au NPs and Au-NC (Figure 3d). At -0.9 V, Au-PANI exhibited a j_{CO} of 11.6 mA cm^{-2}, which was about four times higher than that of Au-NC (2.18 mA cm^{-2}) and seven times higher than that of Au NPs (1.4 mA cm^{-2}). The synthesized Au NPs with an average size of ~10 nm displayed a low current density may be attributed to the low number of active sites available. It has been reported that Au NPs in size of more than 8 nm exhibit a low current density[34]. Our results are comparable to the reported current density of 0.35 mA cm^{-2} at -0.5 V for Au NPs with an average size of more than 20 nm[35] and -1.3 mA cm^{-2} at -0.7 V for Au NPs with an average size of more than 9 nm.[36] It further evidences the critical role of PANI in the Au-PANI composite for CO_2 reduction. More specifically, PANI can effectively trap gaseous CO_2 by interaction to the amine groups in PANI through interaction with the N lone pair to create a new σ-electron bond.

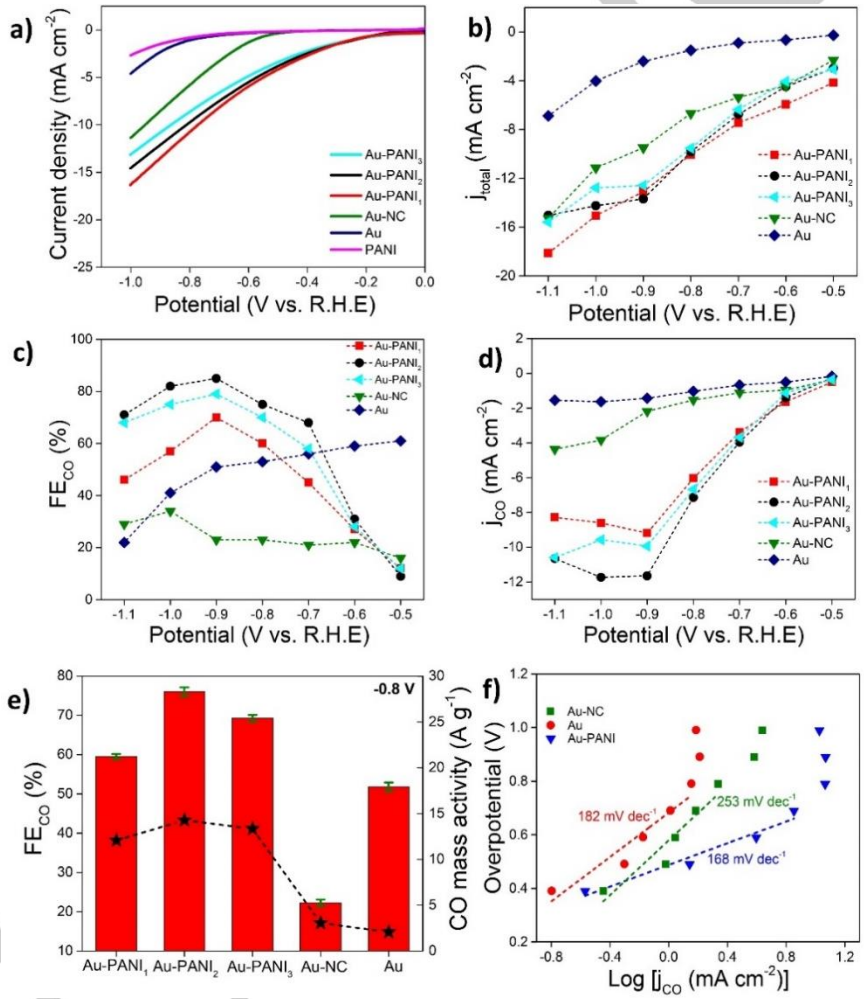

Figure 3. Electrochemical CO_2 reduction performance in CO_2-saturated 0.1 M $KHCO_3$. a) LSV scans of PANI, Au, Au-NC and Au-PANI at a scan rate of 1 mVs^{-1}; (b-d) Geometric total current densities (b), FE_{CO} (c) and j_{CO} (d) at various potentials for all Au-PANI, Au-NC and Au catalysts; (e-f) FE_{CO} (column) and CO mass activity at -0.8 V (e) and Tafel plots (f) of Au-$PANI_2$, Au and Au-NC catalysts for CO production.

The synergistic interaction between Au and PANI promotes the catalytic activity of Au-PANI nanocomposites for CO2 reduction via facilitating CO2 adsorption and stabilizing reaction intermediate (*COOH) on negatively charged Au center, which is realized through the direct axial coordination of amino groups to the gold catalytic centre via strong σ-electron donation. As a result, the CO_2 activation on the metal centre is facilitated, and the formation of CO follows the metal centred reaction mechanism via nucleophilic attack of the centre on the CO_2 molecule due to the higher electron density on the metal centre provided by PANI.[18]

Mass activity is one of the most influential parameters for noble metallic catalysts in terms of their feasibility for large-scale application. Figure 3e highlights the FE_{CO} and CO mass activities

of all Au-PANI nanocomposites, Au-NC and Au at -0.8 V. Au-$PANI_2$ showed a 76% faradaic efficiency for CO production whereas Au and Au-NC displayed a 53% and 23%, respectively. It further distinctly unveils the promoted catalytic effect of PANI on Au. Au-$PANI_2$ displayed high mass activities for the CO_2-to-CO conversion at moderate overpotentials ranging from -0.7 to -0.9 V. For example, a mass activity of 14.2 A g^{-1} at -0.8 V outperformed that reported (6 A g^{-1}) on 4 nm Au NPs on carbon black.[10a]

To gain an understanding about the underlying mechanism of CO formation on these electrodes, Tafel plots were performed (Figure 3f, Figure S5b). Au-$PANI_2$ exhibited a slope of 168 mV dec^{-1}, which indicates that the initial single-electron transfer forming $CO_2^{\bullet-}$ intermediates is the rate-determining step for CO_2-to-CO conversion. In contrast, Au NPs and Au-NC respectively demonstrated a much higher slope of 288 mV dec^{-1} and 345 mV dec^{-1}, evidencing their sluggish kinetics. The improved kinetics for CO formation on Au-PANI may be mainly attributed to the enhanced adsorption of CO_2 from the support of polyaniline and subsequently the formation of *COOH intermediates and fast desorption of CO due to the weak binding of *CO.[18]

The stability of the best performing Au-$PANI_2$ nanocomposite for CO_2ER was investigated at -0.65 V (Figure S6a). It showed a stable current density during the 8 h electrolysis with a slightly increased FE_{CO} in the first 2 h from 68% to 70%. This slight increase may be ascribed to the improved accessibility of electrolyte containing reactants (proton and CO_2) to the active sites. The increased concentration of cations (H^+ and K^+) generated by the electric field during the CO_2 reduction process may contribute as well.[37] Whereas, Au-NC and Au displayed a descending current density and FE_{CO} throughout 5 h and 6 h electrolysis (Figure S6a), respectively. The initial current density of Au-NC was 3 mA cm^{-2} and dropped to 2.3 mA cm^{-2}; while the FE_{CO} decreased from 27% to 20%. Au NPs exhibited an initial current density and FE_{CO} of 0.37 mA cm^{-2} and 57%, and dropped to 0.29 mA cm^{-2} and 50%. These results clearly demonstrate the influence of polyaniline on the stability of the composite catalysts as well. PANI layer on the gold core facilitates the charge transfer and improve the stability of the metallic centre via weakened binding of *CO. It should be noted that the Au-PANI catalyst did not exhibit good stability at a more negative potential of -0.90 V (Figure S6b), suggesting the instability of such small Au NPs under high overpotentials; this phenomenon has been reported for different catalysts including Au NPs stabilized with citrate.[16, 38]

Conclusion

In summary, a shape tailored gold-polyaniline nanocomposite electrocatalyst is synthesized via a single-step method. It is in a core-shell structure with gold as the core and PANI as the shell. The formation of this nanocomposite proceeds through the redox reaction between aniline monomer and gold salt; and is influenced by the ratio between reactants. This catalyst has been used to catalyse CO_2 reduction with high selectivity and acivity. The interaction between Au NPs and amine links in PANI through σ electron donation facilitates CO_2 adsorption and stabilizes the reaction intermediate *COOH. Hence, the introduction of PANI on Au NPs significantly promotes conversion of CO_2-to-CO. The soft nature of PANI with excellent tenability facilitates the formation of composites with a variety of metals.[39] Therefore, this work may motivate the development of core-shell structured conducting polymer/metal nanoparticles as catalysts for CO_2ER.

Experimental

Materials: Aniline monomer (≥ 99.5%, ACS reagent), gold (III) chloride trihydrate ($HAuCl_4 \cdot 3H_2O$, ≥ 99.9%), potassium bicarbonate ($KHCO_3$, ≥ 99.95%), ammonium peroxidodisulfate (APS), sodium borohydride ($NaBH_4$) and Nafion® 117 solution (5 wt%) were purchased from Sigma-Aldrich. Carbon paper (SIGRACET® GDL 38AA, 225 ± 30 µm) was purchased from SGL Carbon GmbH. Ultrapure Milli-Q water (18.2 MΩ·cm) was used in this work.

Materials synthesis and electrode fabrication

Synthesis of gold nanoparticles (Au NPs): This synthesis was performed by adopting a previously reported method.[40] Typically, $HAuCl_4$ solution (200 µL, 0.1M) was added into Milli-Q water (100 mL) and mixed, followed by the slow addition of $NaBH_4$ solution (0.13 M, 5 mL) accompanied by a colour change from yellowish to ruby red. The formed product was collected by filtration, washed with deionized water, then vacuum dried at 60 °C for 24 h to obtain gold nanoparticles (Au NPs).

Synthesis of PANI: A common chemical synthesis method was applied. Briefly, aniline monomer (16 mmol) and ammonium persulfate (APS, 4 mmol) were separately dispersed in a HCl aqueous solution (1 M, 50 mL). Then these two solutions were quickly mixed and kept in an ice bath (0 °C) for 24 h under continuous stirring at 1000 rpm. The colour of the solution changed from light yellow to dark green. After the reaction, the solution was filtered and solids were collected, followed by a rinsing process with water and a drying process in a vacuum oven at 60 °C overnight.

Synthesis of gold-polyaniline (Au-PANI): The reported procedure by Wang et al.[25] was adopted. Briefly, aniline monomer (0.18 ml) was added into Milli-Q water (20 ml), followed by the addition of $HAuCl_4$ aqueous solution (0.1 M, 0.2 ml). This mixture was kept under stirring for 16 h at room temperature. The formed product was collected by filtration and washed with deionized water and ethanol until the filtrate became colourless, and then vacuum-dried at 60 °C for 24 h to obtain Au-PANI nanocomposites.

Carbonisation of Au-PANI nanocomposites : Au-PANI nanocomposites were heated to 800 °C at a rate of 5 °C/min and held at 800 °C for 3 hours in N_2 atmosphere to form Au-N-doped carbon composite (Au-NC).

Fabrication of working electrode. Catalyst inks were prepared by mixing the catalysts (Au-PANI, Au-NC and Au NPs; 60 wt%) and carbon black (Vulcan XC72, 40 wt%) with Nafion solution as the binder in a 50/50 solvent mixture of water and isopropanol. The above mixture was sonicated for 30 min, and then drop cast onto carbon paper (1 cm × 1 cm). Au-PANI electrodes were kept at 60 °C for 20 h in a vacuum oven. The loading mass of Au-PANI composite catalyst was about 0.5 mg cm^{-2}.

Materials Characterisation

Structural Characterization: Crystal structure was analysed by X-ray diffraction (XRD, GBC MMA diffractometer) with Cu Kα radiation at a scan rate of 3 degrees min^{-1}. Morphology was investigated by field emission scanning electron microscopy (FESEM, JEOL JSM-7500FA) and transmission electron microscopy (TEM, JEOL 2010). Dark field STEM imaging was performed on a JEOL JEM-ARM200f. X-ray photoelectron spectroscopy (XPS) spectra were collected by an SES2002 analyser (Scienta) with X-ray excitation from Al Kα radiation (hv = 1486.6 eV). The XPS binding energy spectra were recorded in the fixed analyser transmission mode at a pass-energy of 20 eV. All the spectra were calibrated by C1s = 284.6 eV. Raman spectra were performed with a confocal Raman spectrometer (Jobin Yvon HR800, Horiba) using a 632.8 nm diode laser. Thermal gravimetric analysis (TGA) was performed using a Pyris Diamond thermogravimetric/differential thermal analyser at a heating rate of 10 $^{o}C\ min^{-1}$ in air flow.

Electrochemical measurements: All the experiments were carried out in a gas-tight two-compartment glass H-cell. The cathodic and anodic compartments were separated by Nafion membrane. Each compartment of the cell held 30 mL of electrolyte with a headspace of ~20 mL. A piece of platinum gauze (1.5 cm × 1.5 cm) and an Ag/AgCl (3 M NaCl, BASi) electrode served as counter electrode and reference electrode. A 0.1 M $KHCO_3$ aqueous solution was used as electrolyte directly without any purification. Automatic iR compensation function on the potentiostat (CHI 650D) was used to correct all the potentials. The potentials measured against Ag/AgCl reference electrode were converted to the reversible hydrogen electrode (RHE) scale using the following equation, $E_{RHE} = E_{Ag/AgCl} + 0.21 + 0.0591 \times pH$. The pH of the CO_2-saturated 0.1 M $KHCO_3$ was 6.8. The current density reported in this work was normalized to geometric area.

Prior to the CO_2 reduction reaction, the catholyte was saturated with CO_2 (99.99%, BOC Australia) for at least 30 min under a constant stirring rate of 700 rpm at a flow rate of 20.0 mL min^{-1} controlled by a mass flow controller (GFC17, Aalborg®). Gas CO_2 was continuously bubbled into the cathodic compartment and vented directly into the gas-sampling loop (1 mL) of a gas chromatograph (GC, SRI8610C) during the chronoamperometric electrolysis. This GC was equipped with two packed columns of Mol Sieve 5A and Haysep D with argon as the carrier gas. A thermal conductivity detector (for H_2) and a flame ionization detector with methanizer (for CO, CH_4, and C_2H_4) were used to analyse the gases. Quantification of the products was done by an external standard method, using a standard gas mixture of H_2, CO, CH_4, C_2H_4, C_2H_6 and CO_2 to obtain the calibration curve for each component. The first GC run was started at the 10^{th} min, and thereafter re-started every 16 min twice. The average of results from three measurements was used in the data analysis. Faradaic Efficiencies (FEs) of each product were calculated from the amount of charge passed to produce each product divided by the total charge passed at a specific time.

Acknowledgements

Funding from the Australian Research Council Centre of Excellence Scheme (CE 140100012) is acknowledged. The authors thank Australian National Fabrication Facility-Materials Node (ANFF) and UOW Electron Microscopy Centre for equipment use.

Keywords: Carbon Dioxide Reduction • Catalyst • Gold • Nanocomposite • Polyaniline

1] a) M. Aresta, A. Dibenedetto, *Dalton Trans.* **2007**, 2975-2992; b) H. Arakawa, M. Aresta, J. N. Armor, M. A. Barteau, E. J. Beckman, A. T. Bell, J. E. Bercaw, C. Creutz, E. Dinjus, D. A. Dixon, *Chem. Rev.* **2001**, *101*, 953-996.

[2] S. N. Habisreutinger, L. Schmidt-Mende, J. K. Stolarczyk, *Angew. Chemie* **2013**, *52*, 7372-7408.

[3] A. M. Appel, J. E. Bercaw, A. B. Bocarsly, H. Dobbek, D. L. DuBois, M. Dupuis, J. G. Ferry, E. Fujita, R. Hille, P. J. Kenis, *Chem. Rev.* **2013**, *113*, 6621-6658.

[4] W. Wang, S. Wang, X. Ma, J. Gong, *Chem. Soc. Rev.* **2011**, *40*, 3703-3727.

[5] G. A. Ozin, *Adv. Mater.* **2015**, *27*, 1957-1963.

[6] a) A. S. Agarwal, Y. Zhai, D. Hill, N. Sridhar, *ChemSusChem* **2011**, *4*, 1301-1310; b) J. Qiao, Y. Liu, F. Hong, J. Zhang, *Chem. Soc. Rev.* **2014**, *43*, 631-675.

[7] a) A. S. Varela, W. Ju, T. Reier, P. Strasser, *ACS Catal.* **2016**, *6*, 2136-2144; b) W. Luo, X. Nie, M. J. Janik, A. Asthagiri, *ACS Catal.* **2015**, *6*, 219-229.

[8] a) Y. Hori, in *Mod. Aspects Electrochem.*, Springer, **2008**, pp. 89-189; b) J. Schneider, H. Jia, J. T. Muckerman, E. Fujita, *Chem. Soc. Rev.* **2012**, *41*, 2036-2051.

[9] Y. Chen, C. W. Li, M. W. Kanan, *J. Am. Chem. Soc.* **2012**, *134*, 19969-19972.

[10] a) W. Zhu, R. Michalsky, Ö. Metin, H. Lv, S. Guo, C. J. Wright, X. Sun, A. A. Peterson, S. Sun, *J. Am. Chem. Soc.* **2013**, *135*, 16833-16836; b) H.-E. Lee, K. D. Yang, S. M. Yoon, H.-Y. Ahn, Y. Y. Lee, H. Chang, D. H. Jeong, Y.-S. Lee, M. Y. Kim, K. T. Nam, *ACS nano* **2015**, *9*, 8384-8393; c) W. Zhu, Y.-J. Zhang, H. Zhang, H. Lv, Q. Li, R. Michalsky, A. A. Peterson, S. Sun, *J. Am. Chem. Soc.* **2014**, *136*, 16132-16135.

[11] a) Y. Fang, J. C. Flake, *J. Am. Chem. Soc.* **2017**, *139*, 3399-3405; b) K.-S. Kim, W. J. Kim, H.-K. Lim, E. K. Lee, H. Kim, *ACS Catal.* **2016**, *6*, 4443-4448.

[12] a) K. Chen, X. Zhang, T. Williams, L. Bourgeois, D. R. MacFarlane, *Electrochim. Acta* **2017**, *239*, 84-89; b) Z. Xu, E. Lai, Y. Shao-Horn, K. Hamad-Schifferli, *Chem. Commun.* **2012**, *48*, 5626-5628; c) C. Hahn, D. N. Abram, H. A. Hansen, T. Hatsukade, A. Jackson, N. C. Johnson, T. R. Hellstern, K. P. Kuhl, E. R. Cave, J. T. Feaster, *J. Mater. Chem. A* **2015**, *3*, 20185-20194.

[13] a) H.-L. Jiang, Q. Xu, *J. Mater. Chem.* **2011**, *21*, 13705-13725; b) C. Rogers, W. S. Perkins, G. Veber, T. E. Williams, R. R. Cloke, F. R. Fischer, *J. Am. Chem. Soc* **2017**, *139*, 4052-4061; c) Y. Mun, K. Kim, S. Kim, S. Lee, S. Lee, S. Kim, W. Choi, S.-k. Kim, J. W. Han, J. Lee, *Appl. Catal., B* **2018**, *236*, 154-161.

[14] Q. Li, W. Zhu, J. Fu, H. Zhang, G. Wu, S. Sun, *Nano Energy* **2016**, *24*, 1-9.

[15] M. Cho, J.-W. Seo, J. T. Song, J.-Y. Lee, J. Oh, *ACS Omega* **2017**, *2*, 3441-3446.

[16] Y. Zhao, C. Wang, Y. Liu, D. R. MacFarlane, G. G. Wallace, *Adv. Energy Mater.* **2018**, 1801400.

[17] T. P. Farrell, R. B. Kaner, in *Encyclopedia of Polymeric Nanomaterials* (Eds.: S. Kobayashi, K. Müllen), Springer Berlin Heidelberg, Berlin, Heidelberg, **2021**, pp. 1-8.

[18] S. Ponnurangam, I. V. Chernyshova, P. Somasundaran, *Adv. Colloid Interface Sci.* **2017**, *244*, 184-198.

[19] W. Zheng, S. Nayak, W. Yuan, Z. Zeng, X. Hong, K. A. Vincent, S. C. E. Tsang, *Chem. Commun.* **2016**, *52*, 13901-13904.

[20] C. Zhao, Z. Yin, J. Wang, *ChemElectroChem* **2015**, *2*, 1974-1982.

[21] A. N. Grace, S. Y. Choi, M. Vinoba, M. Bhagiyalakshmi, D. H. Chu, Y. Yoon, S. C. Nam, S. K. Jeong, *Appl. Energy* **2014**, *120*, 85-94.

[22] F. Li, *Electrochim. Acta* **2020**, *332*, 135457.

[23] a) J. Song, J. Yuan, F. Li, D. Han, J. Song, L. Niu, *J. Solid State Electrochem.* **2010**, *14*, 1915-1922; b) U. Bogdanović, I. Pašti, G. Ciric-Marjanovic, M. Mitrić, S. P. Ahrenkiel, V. Vodnik, *ACS Appl. Mater. Interfaces* **2015**, *7*, 28393-28403.

[24] a) D. Li, C. Wang, D. Tripkovic, S. Sun, N. M. Markovic, V. R. Stamenkovic, *ACS Catal.* **2012**, *2*, 1358-1362; b) Q. Xu, J. Leng, H.-b. Li, G.-j. Lu, Y. Wang, X.-Y. Hu, *React. Funct. Polym.* **2010**, *70*, 663-668; c) S. Ivanov, U. Lange, V. Tsakova, V. M. Mirsky, *Sens. Actuators, B* **2010**, *150*, 271-278; d) J. Han, M. Wang, Y. Hu, C. Zhou, R. Guo, *Prog. Polym. Sci.* **2017**, *70*, 52-91.

[25] X. Wang, Y. Shen, A. Xie, S. Li, Y. Cai, Y. Wang, H. Shu, *Biosens. Bioelectron.* **2011**, *26*, 3063-3067.
[26] a) W. Qiu, H. Huang, S. Zeng, T. Xue, J. Liu, *J. Polym. Res.* **2011**, *18*, 19-23; b) J. M. Kinyanjui, D. W. Hatchett, J. A. Smith, M. Josowicz, *Chem. Mater.* **2004**, *16*, 3390-3398.
[27] H. HianáTeo, *Chem. Commun.* **2010**, *46*, 7112-7114.
[28] a) X. Feng, C. Mao, G. Yang, W. Hou, J.-J. Zhu, *Langmuir* **2006**, *22*, 4384-4389; b) L. Zhang, M. Wan, *Adv. Funct. Mater.* **2003**, *13*, 815-820.
[29] a) M. Xin, H. Lin, J. Yang, M. Chen, X. Ma, J. Liu, *Electroanalysis* **2014**, *26*, 2216-2223; b) X. Feng, G. Yang, Q. Xu, W. Hou, J.-J. Zhu, *Macromol. Rapid Commun.* **2006**, *27*, 31-36.
[30] R. J. Tseng, C. O. Baker, B. Shedd, J. Huang, R. B. Kaner, J. Ouyang, Y. Yang, *Appl. Phys. Lett.* **2007**, *90*, 053101.
[31] a) L. Shi, Z. Wang, G. Yang, X. Chen, G. Gou, W. Liu, *Electrochemistry* **2017**, *85*, 384-390; b) S. Liu, H. Xu, J. Ou, Z. Li, S. Yang, J. Wang, *Mater. Chem. Phys.* **2012**, *132*, 500-504.
.
[32] L. Zhang, H. Peng, P. A. Kilmartin, C. Soeller, R. Tilley, J. Travas-Sejdic, *Macromol. Rapid Commun.* **2008**, *29*, 598-603.
[33] A. B. Afzal, M. J. Akhtar, M. Nadeem, M. Hassan, *J. Phys. Chem. C* **2009**, *113*, 17560-17565.
[34] T. Zheng, K. Jiang, H. Wang, *Adv. Mater.* **2018**, *30*, 1802066.
[35] H. Mistry, R. Reske, Z. Zeng, Z.-J. Zhao, J. Greeley, P. Strasser, B. R. Cuenya, *J. Am. Chem. Soc.* **2014**, *136*, 16473-16476.
[36] S. Chen, A. Chen, *J. Phys. Chem. C* **2019**, *123*, 23898-23906.
[37] Y. Zhao, J. Liang, C. Wang, J. Ma, G. G. Wallace, *Adv. Energy Mater.* **2018**, *8*, 1702524.
[38] J. A. Trindell, J. Clausmeyer, R. M. Crooks, *J J. Am. Chem. Soc.* **2017**, *139*, 16161-16167.
[39] D. W. Hatchett, M. Josowicz, *Chem. Rev.* **2008**, *108*, 746-769.

Table of Contents

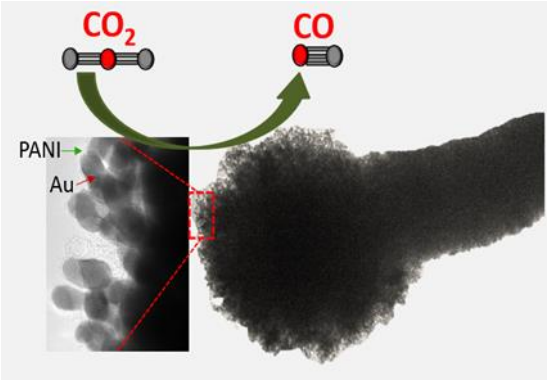

Core-shell structured gold-polyaniline nanocomposite in shape tailored posy bouquet morphology is synthesized via a self-induced redox reaction. It demonstrates an excellent electrocatalytic activity towards the CO_2-to-CO conversion. The PANI shell plays a critical role in catalysing the CO_2 reduction.